Thermal quench runaway electron generation and post current quench runaway deconfinement characteristics

A.N. James[1], E.M. Hollmann[1], N. Eidietis[2], D.A. Humphreys[2], P.B. Parks[2], E.J. Strait[2], G.R. Tynan[2], J.C. Wesley[2]

[1] *University of California San Diego, La Jolla, USA*

[2] *General Atomics, San Diego, USA*

The significant loop voltages induced during rapid-shutdowns and disruptions of tokamaks can generate runaway electrons which then may damage machine components. We present results from a new spatially distributed scintillator array designed for observing the spatial distribution of x-rays emitted by runaway deconfinement and also for rough energy resolution. Using this array we describe multiple phases of runaway electron deconfinement with various generation and deconfinement mechanisms governing the evolution throughout. To explain the early presence of runaway electrons before current quench loop voltages could accelerate them, we also discuss analysis of internal loop voltages which reveals a previously neglected early loop voltage not captured by poloidally averaged external measurements.

Thermal quench

Using a new hard x-ray sensitive scintillator array [1] and existing soft x-ray arrays, we observe runaway electrons with 1-5MeV energy impacting the divertor after the thermal quench but before the current quench begins, shown in figure 1. To begin, we induce rapid shutdowns of otherwise stable plasmas using injected argon ice pellets, which radiate strongly and cause a thermal collapse resulting in a drop of plasma cyclotron and thermal x-ray emission, shown in figure 1a and b, and c respectively. As shown previously, shutdowns utilizing these argon pellets generate a larger magnitude of runaway electron current more consistently than other techniques [2]. Just after thermal emission subsides, an x-ray burst appears at the inner strike point where positively charged particles (ions or positrons) would strike if accelerated along magnetic field lines by inductive

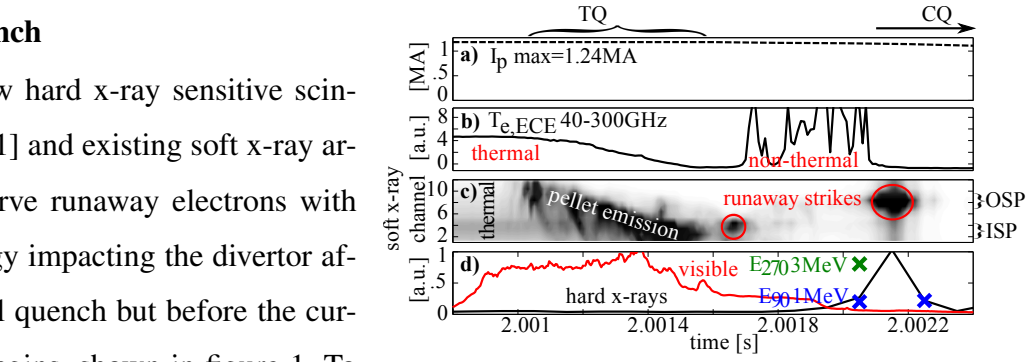

Figure 1: Data observed during a thermal quench including: a) plasma current I_p, b) thermal and non-thermal cyclotron emission, c) soft x-ray array showing thermal emission, pellet line radiation, and bremsstrahlung emission from runaways striking the divertor at the inner and outer strike points (ISP and OSP respectively), and d) visible emission from the pellet, hard x-ray emission, and runaway energy inferred from the scintillator array. Temporal phases including the thermal quench (TQ) and current quench (CQ) are indicated along the top.

loop voltages, though this emission was previously attributed [3] to runaway electrons striking argon in the plasma core. After the temperature drop indicated by decay of thermal cyclotron emission, non-thermal bursts occur possibly due to knock-on electrons with high energy perpendicular to the magnetic field [4] created by accelerating runaways, though only a small loop voltage from dropping plasma current occurs at this time. Shortly after non-thermal cyclotron emission subsides, soft x-ray array chords viewing the outer strike point briefly detect a burst of x-rays and nearby scintillators observe hard x-ray emission, both associated with energetic de-confined runaway electrons striking the divertor. The scintillator array also observes toroidal asymmetry of this strike which is consistent between shots. By using the code EGSnrc [5] to model the x-ray absorption in scintillators wrapped in different thicknesses of lead, and matching this model to the observed x-ray attenuation between detectors, we infer a runaway electron energy of 1-5MeV during this initial thermal quench phase. Observed non-thermal cyclotron emission and subsequent soft and hard x-ray observations occur before external sensors measure any loop voltage associated with changes in current, suggesting the presence of some unseen loop voltage.

Loop voltages during thermal quench

With the magnetic reconstruction code JFIT [6], we track current motion in the plasma region, and hence the evolving loop voltages induced as the inductance and current change in time, shown in figure 2. JFIT solves for distributed current elements on a grid using only magnetic measurements made near the wall for inputs. It is not constrained for Grad-Shafranov equilibrium solutions, but this ensures convergence even during dynamic situations such as disruptions when equilibrium solvers like EFIT either fail or barely converge. Using the magnetic fields B_p generated by these in-vessel currents I_p, we calculate the inductance as $L_{int} = \frac{1}{\mu_0 I_p^2} \int B_p^2 dV$. The integral is done only internally over the plasma region defined by the first wall, neglecting external contributions which should only come into play on timescales longer than the wall current time. The resulting inductance drops faster than a 1D model L_{Parks} based on the plasma major radius, which neglects current profile flatten-

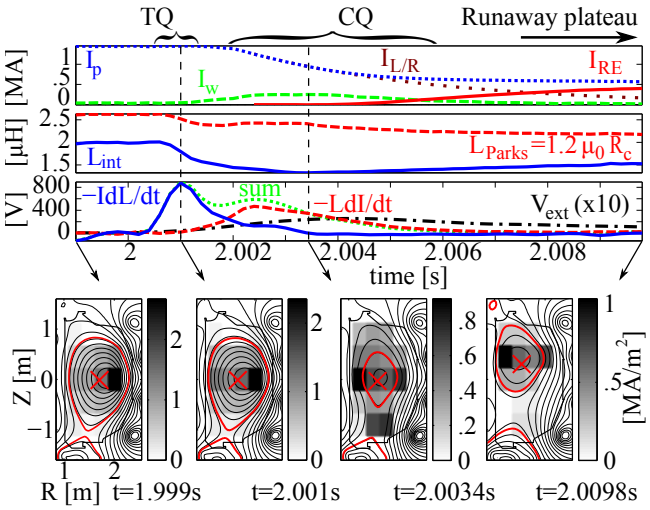

Figure 2: JFIT analysis of loop voltages spanning the thermal quench and current quench phases showing total measured current I_p, wall current I_w calculated by the difference of total current measured inside and outside the vessel, runaway electron current I_{RE} calculated by the difference of total current and an L/R current decay $I_{L/R}$ fit at the maximum of $\frac{dI_p}{dt}$, calculated inductance L_{int}, and finally loop voltages calculated from these. Below are coarse grid current distributions solved by JFIT at four times, with resulting flux contours.

ing. From this evolving inductance, we calculate the in-vessel loop voltage accounting for both changes in inductance and current:

$$V_{loop} = -\frac{d}{dt}(LI) = -I\frac{dL}{dt} - L\frac{dI}{dt} \quad (1)$$

During the thermal quench phase, the often neglected first term in equation 1 dominates due to a drop in inductance from rapid current motion toward smaller major radius and current profile flattening. This term is not captured by 0D external loop voltage measurements (V_{ext} in figure 2), and hence must be calculated using magnetic sensors distributed around the poloidal circumerence to invert the current topology. It is also larger in magnitude and occurs roughly 1ms earlier than the second term when the temperature is higher and density is lower, all of which increase the normalized electric field $\varepsilon = E_\phi/E_D$ for runaway seed generation via the Dreicer mechanism where $E_D = \frac{e^3 ln\Lambda}{4\pi\varepsilon_0^2}\frac{n_e}{kT_e}$, and the runaway electron production rate [7, 4] is

$$\gamma_D = \frac{1}{n_e}\frac{dn_{RE}}{dt} = A(Z_{eff})\varepsilon^{-(Z_{eff}+1)3/16}\nu_{ee}e^{-1/4\varepsilon-\sqrt{(Z_{eff}+1)/\varepsilon}} \quad (2)$$

The enhanced early loop voltage revealed by this analysis suggests greater significance of the runaway electron generation mechanism proposed by Dreicer than would be possible from the current drop term.

Current quench

After the thermal quench subsides and the current quench begins, runaway current increases to less than half of the initial current magnitude and the average energy measured by the scintillator array rises slowly, shown in figure 3a and b, but remains below a theoretical maximum for luminal electrons falling down the loop voltage without drag $\varepsilon = \int \frac{ecV_{loop}}{2\pi R}dt$. The new scintillator array observes x-ray emission along the midplane (figure 4b) which gradually increases with runaway current during the subsequent current plateau, which sometimes lasts for 100s of milliseconds.

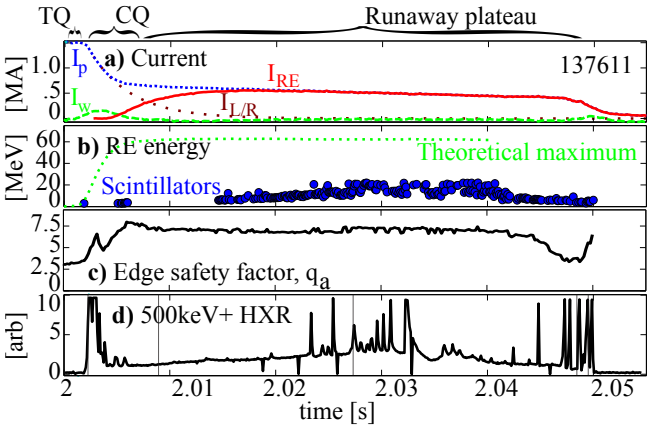

Figure 3: Data observed during the current quench and plateau phases including a) currents, b) runaway energy measured with scintillators and a theoretical maximum, c) the edge safety factor calculated [8] by JFIT, and d) hard x-ray emission measured by a midplane detector at 90 degrees toroidal.

During this long plateau phase, numerous brief intense bursts of x-ray emission occur, shown in figure 3d. The scintillator array observes these x-ray bursts at the midplane and ceiling, but not along the floor (shown in figure 4c), suggesting that they result from intermittent impact of runaways along the ceiling, perhaps due to current filaments separating through magnetic

turbulence [9].

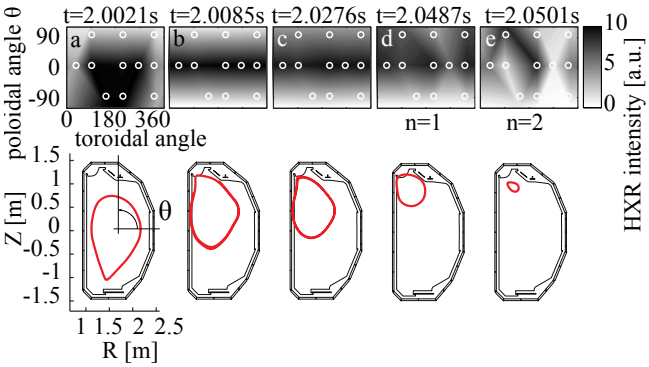

Figure 4: Spatial hard x-ray emission profiles with detector locations circled and JFIT magnetic reconstructions of last closed flux surface location.

The plateau terminates generally in one of two typical scenarios from the perspective of the edge safety factor q_a: either it drops toward the end resulting in a presumed ideal kink instability (as in figure 3c), or it gradually rises corresponding to a limiting surface slowly peeling off current. Toroidal asymmetries of n=1 and n=2 character also occur on the scintillator array in the case when q_a drops as shown in figure 4d and e, further supporting the cause as a kink instability.

Summary

Based on experimental observations using a new scintillator array, we have identified anomalously high energy runaway electrons after the thermal quench, indicating the presence of some accelerating voltage before the inductive loop voltage associated with current quench begins. To explore possible voltage sources, we performed thorough analysis of magnetic data using the code JFIT which reveals an enhanced early loop voltage from an inductance drop due to current profile motion and flattening. This enhanced loop voltage results in an enhanced contribution of the Dreicer effect for runaway electron generation. Observations of multiple phase runaway deconfinement during the current plateau phase suggest the activity of intermittent transport processes and ideal instabilities, indicating consideration for these stability criteria to maintain runaway confinement and prevent damage to first wall components.

References

[1] A. N. James 2010 *Submitted to Review of Scientific Instruments*

[2] T. E. Evans 1998 *Proc. of the 17th IAEA FEC* **3** 847

[3] E. M. Hollmann 2005 *Nucl. Fus.* **45** 1046–1055

[4] R. Jayakumar, H. H. Fleischmann, S. J. Zweben 1993 *Physics Letters A* **172** 447 – 451 ISSN 0375-9601

[5] I. Kawrakow 2009 *NRCC Report* **PIRS-701**

[6] D. A. Humphreys, A. G. Kellman 1999 *Physics of Plasmas* **6** 2742–2756

[7] H. Dreicer 1959 *Phys. Rev.* **115** 238–249

[8] J. P. Freidberg 1987 *Ideal Magnetohydrodynamics* (New York: Plenum Press) chap 12, p 112

[9] A. B. Rechester 1978 *Phys. Rev. Lett.* **40** 38–41